

## Direct detection of the non-thermal X-ray emission from the Arches star cluster

Roman Krivonos<sup>1\*</sup>, Alexey Vikhlinin<sup>2,1</sup>, Andrei Bykov<sup>3</sup>,  
Sergey Sazonov<sup>1</sup> and Maïca Clavel<sup>4</sup>

<sup>1</sup>Space Research Institute, Russian Academy of Sciences, Moscow, 117997 Russia

<sup>2</sup>Center for Astrophysics | Harvard & Smithsonian, 60 Garden St, Cambridge, MA, USA

<sup>3</sup>Ioffe Institute, Politekhnicheskaya str., 26, St. Petersburg, 194021, Russia

<sup>4</sup>Univ. Grenoble Alpes, CNRS, IPAG, Grenoble, 38000, France

Received 28.11.2025

Revised November 28, 2025; Accepted December 1, 2025

**Abstract** — The compact stellar clusters have emerged as particularly promising candidates for cosmic rays (CR) accelerators. The star clusters, recently observed in  $\gamma$ -rays, are also known sources of non-thermal X-ray emission, which is due to synchrotron or inverse-Compton scattering of relativistic electrons. Thus, the search for the non-thermal X-ray emission from stellar clusters is of particular interest. Until recent time the X-ray emission of the Arches star cluster in the Galactic Center was mixed with non-thermal emission of the surrounding molecular cloud, associated with reflection of hard X-ray irradiation. This reflected emission has been observed to fade, giving us a chance to characterize intrinsic non-thermal emission of the Arches cluster. In this work we demonstrate that Fe K $\alpha$  line emission at 6.4 keV, attributed to the reflected non-thermal emission of the molecular cloud in 2000–2010, is not detected in deep observations with XMM-Newton in 2020 and Chandra in 2022, leaving stellar cluster well isolated. We showed that the Arches non-thermal emission is localized in the cluster's core and characterized by a relatively weak, hard ( $\Gamma \approx 1.5$ ) power-law spectral continuum with 2–10 keV flux of  $\sim 10^{-13}$  erg s $^{-1}$  cm $^{-2}$ .

**Key words:** X-rays: general, Galaxy: bulge, Galaxy: general, gamma rays: diffuse background, X-rays: diffuse background

### INTRODUCTION

The Galactic center (GC) hosts numerous young massive stars, which generate ultraviolet radiation and stellar winds, injecting energy into the interstellar medium (ISM). A significant fraction of these massive early-type stars are hosted in star clusters. There are three main star clusters in the GC: the young nuclear cluster (YNC; Krabbe et al. 1991) which is a part of the Nuclear Stellar Cluster (NSC) but dominates the central parsec, the Arches cluster (Nagata et al. 1995), and the Quintuplet cluster (Nagata et al. 1990). These star clusters are believed to be formed within recent few million years and contain numerous massive stars (Lu et al. 2019).

When massive stars reside in binary systems, the intense stellar winds will collide with each other, forming the so-called colliding-wind binaries. The colliding wind generates strong shocks and produces a hot plasma (with a temperature  $> \sim 10^6$  K). Relativistic particles are also observed in such systems (Eich-

ler & Usov 1993; Stevens 1995), which can be accelerated through diffusive shock acceleration (Drury 1983). These systems can be bright in the X-ray band. X-ray emission has been detected in several objects including Apep (del Palacio et al. 2023), Eta Carinae (Hamaguchi et al. 2018), and  $\gamma$  Vel (Willis, Schild & Stevens 1995). The overall spectral shape of typical colliding wind sources in X-rays contains a soft thermal component as well as a hard non-thermal component. The latter is believed to originate by synchrotron or inverse-Compton scattering of relativistic electrons, which contributes to hard X-rays and even  $\gamma$ -rays. The wind velocity and the post-shock temperature determine the thermal component, which contains a bremsstrahlung continuum and emission lines mainly from the K-shell transitions of various elements.

Detection of very high energy (VHE)  $\gamma$ -rays from clusters of young massive stars (Aharonian et al., 2019), provided evidence that acceleration of Galactic Cosmic Rays (CRs) can take place in compact stellar clusters, which can be considered as very high energy CR factories. Particle acceleration by multiple

\* e-mail: krivonos@cosmos.ru

shocks can raise the maximum energy of CR protons out of 1 PeV, making stellar clusters potential candidates for Galactic PeVatrons, especially when the most massive stars produce core-collapsed supernovae (see e.g. Bykov, 2014).

Deep observations of rich clusters of young massive stars Westerlund 1 and 2 with Chandra (Muno et al., 2006; Townsley et al., 2019) and XMM-Newton (Kavanagh, 2020) detected diffuse X-ray emission from the clusters and their close vicinities. Analysis of X-ray spectra of both clusters provided evidence of the possible presence of non-thermal pow-law components (Muno et al., 2006; Bykov et al., 2023) that can be produced by synchrotron radiation of very high energy electrons. Evidence for non-thermal X-ray emission was found by Sasaki et al. (2022) in eROSITA/SRG spectra of the rich stellar cluster RMC 136 located in the LMC starforming region Doradus 30.

The young, massive Arches star cluster (G0.12+0.02; Cotera et al., 1996; Serabyn et al., 1998) is located about 25 pc in projection from the Galactic center. The cluster has a compact core that is about 9'' ( $\sim 0.35$  pc at 8 kpc) in radius (Figer et al., 1999), with an average mass density of  $\sim 3 \times 10^5 M_\odot \text{ pc}^{-3}$ , containing more than 160 O-type stars (Figer et al., 2002). There are 13 Wolf-Rayet (WR) stars detected in the cluster (e.g., Clark et al., 2018a,b, 2019).

Based on the first serendipitous Chandra observations of the Arches cluster region, Yusef-Zadeh et al. (2002) reported the detection of two bright X-ray sources within the central part of the Arches cluster surrounded by diffuse X-ray emission. Authors found that X-ray emission of these sources coincides with the core of the cluster and can be fitted with a two-temperature thermal spectrum with a soft and hard component. The diffuse emission around the cluster was discussed in the context of combined shocked stellar winds escaping from the cluster.

A number of dedicated X-ray campaigns have been initiated to establish the presence of thermal and non-thermal emission components. The thermal emission is thought to originate from multiple collisions between strong winds of massive stars (Chlebowski & Garmany, 1991; Yusef-Zadeh et al., 2002; Wang et al., 2006; Capelli et al., 2011a). The extended, non-thermal X-ray emission has been detected around the cluster (Wang et al., 2006; Tsujimoto et al., 2007; Capelli et al., 2011b; Tatischeff et al., 2012; Krivonos et al., 2014). The non-thermal origin of diffuse emission was revealed by fluorescent Fe  $K\alpha$  line emission of neutral or low ionized material. The fluorescent emission is produced by ejecting a K-shell electron, either by hard X-ray photoionization from an external X-ray source (reflection mechanism), or by the collisional ionization

Table 1. Log of XMM-Newton observations of the Arches cluster, used in this work.

Date	ObsID	Exp., ks	Offset, '
2020-09-19	0862470701	43	4.14
2020-09-21	0862470601	43	6.36
2020-09-26	0862470801	43	10.37

induced by cosmic-ray (CR)-accelerated electrons or ions (CR-induced scenario).

The mechanism producing the fluorescent line emission around the Arches cluster was not completely understood for a long time. Based on XMM-Newton data, Tatischeff et al. (2012, hereafter T12) argued that bright 6.4 keV line extended emission observed around the Arches cluster is very likely produced by bombardment of molecular gas by energetic ions. This statement was mainly based on apparently constant X-ray flux, however, Clavel et al. (2014) analyzed the long-term behavior of the Arches cluster molecular cloud (or simply the Arches cloud) over 13 yr with XMM-Newton and reported a 30% decrease in Fe  $K\alpha$  line and continuum flux of the cloud emission, providing significant evidence for the X-ray reflection scenario. Later, Krivonos et al. (2017), with long NuSTAR and XMM-Newton observations in 2015 showed that the non-thermal emission of the Arches cloud vanished after 2012, leaving three bright clumps. The declining trend of the cloud emission was consistent with half-life decay time of  $\sim 8$  yr, similar to several other molecular clouds in the Galactic Center.

Thus, the study of the intrinsic non-thermal emission of the Arches star cluster was complicated by presence of the nearby cloud emission. The detection of 6.4 keV line within the cluster points out to this ‘contamination’, e.g. T12 suggested that 6.4 keV line in the cluster’s core is produced in molecular gas along the line of sight outside the star cluster. Therefore, the long-term fading of the Arches cloud (Clavel et al., 2014; Kuznetsova et al., 2019; Stel et al., 2025), opens a possibility to observe intrinsic non-thermal emission of the cluster. The non-detection of 6.4 keV line in the cluster would indicate that possible contribution of the reflected emission is not significant.

In this work we analyze deep and moderately off-axis XMM-Newton observations of the Arches cluster taken in 2020 during Central Molecular Zone (CMZ) survey, with the aim to characterize its intrinsic non-thermal emission, having the fact that the reflected X-ray emission of the surrounding molecular cloud is not significantly detected. Additionally, we utilize Chandra observations of the Arches cluster, taken in 2022 as a part of deep survey of CMZ region (Marin et al., 2023). The paper is organized as follows. Sect. describes the observations and data reduction, including

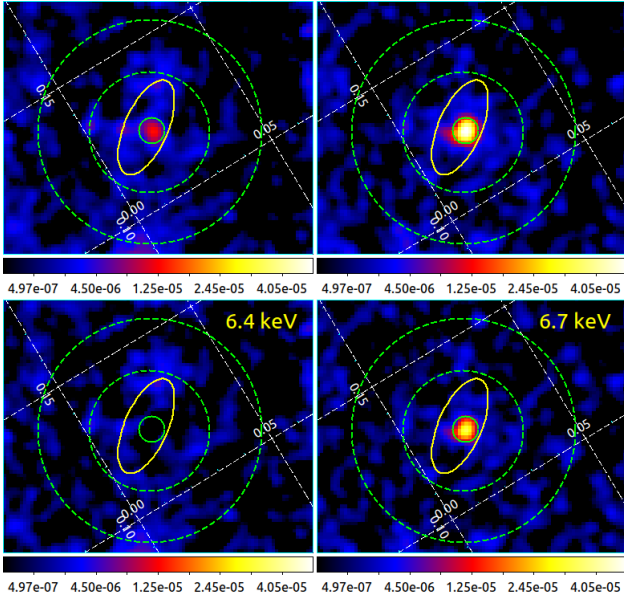


Fig. 1. Upper panels: XMM-Newton/EPIC exposure- and background-corrected maps of the Arches cluster region containing the line (and continuum) emission at 6.4 keV (left panels) and 6.7 keV (right panels) observed in 2020. The images, initially corrected for particle background, were corrected for astrophysical background measured in the green dashed annulus. Bottom panels: sky images, additionally corrected for continuum emission, represent Fe K $\alpha$  emission line maps at 6.4 keV and 6.7 keV. The green circle with radius of 15'' indicates the region used to characterize the Arches cluster X-ray emission, which shows strong Fe K $\alpha$  emission at 6.7 keV. Yellow ellipse denotes reference region of the Arches molecular cloud observed earlier at 6.4 keV, adopted from T12. Green dashed annulus is also used in spectral analysis to extract background. All sky images were convolved with a Gaussian ( $\sigma = 1.5$  pix, the pixel size is 4'').

sky map production and extraction of X-ray spectra. In Sect. we present results for morphology analysis and spectral decomposition of the Arches X-ray emission. Discussion, summary and conclusions are given in Sections -.

## OBSERVATIONS AND DATA REDUCTION

We analyzed deep observations of the Arches cluster region, taken during observational campaigns of CMZ with XMM-Newton in 2020 (PI: Clavel) and Chandra in 2022 (PI: Vikhlinin). We selected only observations with Arches cluster appeared in the field of views's (FOV's) of both observatories. Table 1 contains the list of used XMM-Newton observations in 2020.

### XMM-Newton observations in 2020

The XMM-Newton data reduction was carried out using the XMM-Newton Science Analysis Software (SAS) version 22. Calibrated event files were produced using the tasks emproc for the MOS cameras and epproc for the pn camera. We ex-

cluded from the analysis the period contaminated by soft proton flares using espfilt from the Extended Source Analysis Software (ESAS, Snowden et al., 2004, 2008) package, included in SAS. We selected events with XMMEA\_EM&PATTERN  $\leq 12$  and XMMEA\_EP&PATTERN  $\leq 4$  for MOS cameras and pn instrument, respectively. The particle background was derived from Filter-Wheel Closed (FWC) observations using evqpb task from ESAS. We applied exactly the same event selection criteria to both data and FWC files (see also Sect. ).

Similar to T12, we produced count images in three energy bands 4.17–5.86 keV, 6.3–6.48 keV and 6.564–6.753 keV, which contain the continuum emission, the Fe K $\alpha$  lines at 6.4 keV from neutral to low-ionized atoms and at 6.7 keV from a hot thermally-ionized plasma. For each observation, instrument, energy band, the normalized FWC image was subtracted from the count image. The corresponding vignetting-corrected exposure maps were generated with eexpmap task.

The Arches cluster core emission is embedded in the elongated non-thermal emission of the cloud with dimensions of  $\sim 25 \times 59$  arcsec $^2$ , which approximately corresponds to yellow ellipse in Fig. 1. In order to perform spatial and spectral analysis consistent with other studies of the Arches cluster we adopt the same sky regions to describe the core of the Arches cluster and the surrounding cloud region.

We extracted MOS1, MOS2 and pn spectra for each observation from the Arches cluster core region, described as a circle with radius of 15'', which is selected to cover the compact cluster's core taking XMM-Newton point spread function into account. It also corresponds to the same Arches cluster core region used in T12 and other works (Clavel et al., 2014; Krivonos et al., 2014, 2017; Kuznetsova et al., 2019). The background spectrum was measured in annulus region with internal and outer radius of 70'' and 130'', respectively.

Spectral analysis was done using XSPEC (Arnaud, 1996), setting the atomic cross sections to Verner et al. (1996) and the abundances to (Wilms et al., 2000). We merged MOS1, MOS2 and pn spectra for each observation using epicspeccombine task.

### Chandra observations in 2022

We use Chandra data from deep observations of the CMZ region performed in 2022 with a total exposure of 900 ks. A part of this survey also covers the Arches cluster zone. The detailed description of Chandra observations and the procedure for data analysis can be found in Marin et al. (2023); see also Vikhlinin et al. (2009). For better modeling of the instrumental background, the data have been organized in three epochs 2022-03, 2022-07 and 2022-09. Spectral extraction be-

tween 1 and 9 keV of the Arches cluster emission has been made from the same circular region with  $15''$  radius, used throughout this work.

## RESULTS

### Morphology

In Fig. 1 (upper panel) we show exposure- and FWC- corrected maps of the Arches cluster region in the energy bands containing 6.4 keV and 6.7 keV line emission as observed with XMM-Newton in 2020. The images were additionally subtracted with mean astrophysical background measured in the annulus region. However, in order to produce sky maps of the  $\text{Fe K}\alpha$  emission at 6.4 and 6.7 keV, the underlying continuum needs to be subtracted. To this end, the continuum-dominated 4.17–5.86 keV map was renormalized to the power-law flux in the considered energy band and then subtracted from the corresponding energy band image. We use absorbed power-law model with photon index  $\Gamma = 3$ , consistent with spectral analysis presented below. The resulting continuum-corrected sky images of the Arches complex (Fig. 1, bottom) demonstrate that 6.4 keV  $\text{Fe K}\alpha$  line structures observed around the Arches cluster (inside the reference ellipse region) in 2000–2010 and attributed to the molecular cloud emission are not detected in 2020, including the core of the cluster. This fact is also confirmed by strong suppression of  $\text{Fe K}\alpha$  emission of the cluster region observed in multi-year XMM-Newton maps of the CMZ (Stel et al., 2025). Bright 6.7 keV line emission, as expected, is concentrated in the cluster’s core.

### Spectral analysis

In the Arches cluster region T12 identified an optically thin thermal plasma with a temperature  $kT \sim 1.6\text{--}1.8$  keV and a relatively weak non-thermal component characterized by a hard continuum emission and a line at 6.4 keV from neutral to low-ionized Fe atoms ( $\text{EW}_{6.4 \text{ keV}} = 0.4 \pm 0.1$  keV). T12 suggested that the 6.4 keV line detected from this region is produced in molecular gas along the line of sight outside the star cluster. To test this assumption, we start with constraining non-thermal molecular cloud emission traced by  $\text{Fe K}\alpha$  6.4 keV line in the projected region of the Arches cluster core. To this end, we simplify spectral fitting by limiting energy range to 4–10 keV and considering 6.4 keV and 6.7 keV line emission above the power-law continuum with free photon index and normalization. We used the following model:

$$\text{const} \times (wabs \times \text{pegpwrlw} + \text{gaussian} + \text{gaussian}) \quad (1)$$

where *const* term describes cross-normalization between different observations; *wabs* is an absorption

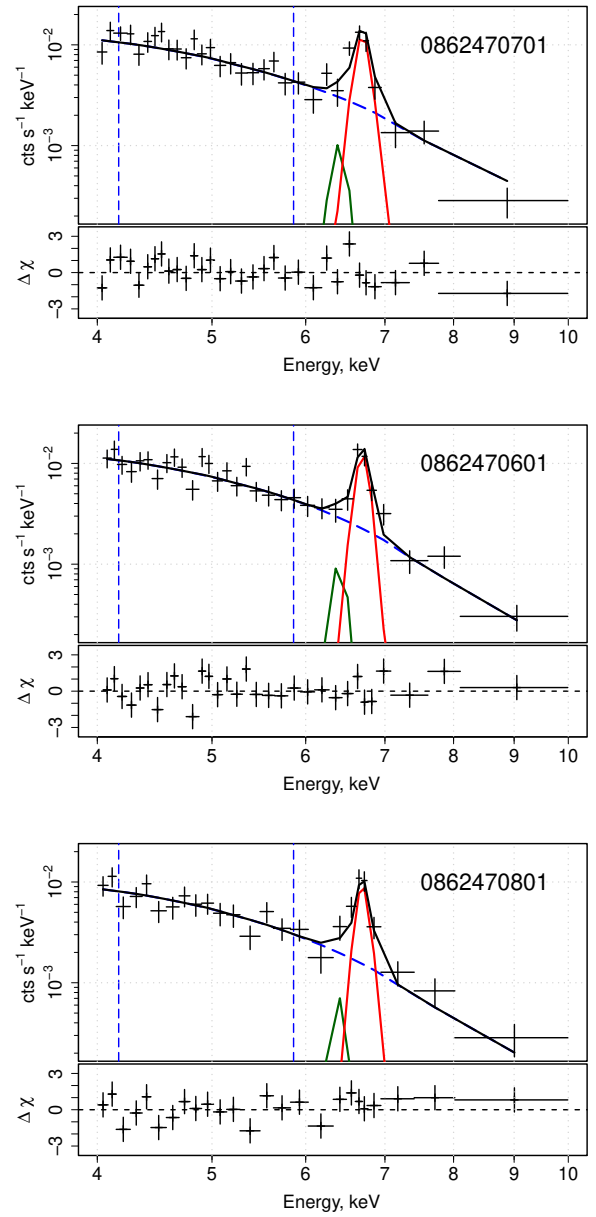


Fig. 2. Merged MOS1, MOS2 and pn X-ray spectra of the Arches cluster between 4 and 10 keV for three XMM-Newton observations in 2020. Best-fitting model (solid black line) is composed by a combination of an absorbed power-law (dashed blue) normalized in energy range shown by vertical blue dashed lines, and two Gaussian functions attributed to  $\text{Fe K}\alpha$  lines at 6.4 keV (dark green) and 6.7 keV (red).

Table 2. Best-fitting parameters of a power-law model (Eq. 1).

Parameter	Units	XMM-Newton 2020		Chandra 2022	
		ObsID	Value	Epoch	Value
<i>const</i>		0862470701	1.0 (fixed)	2022-03	1.0 (fixed)
<i>const</i>		0862470601	1.18 ± 0.11	2022-07	1.01 ± 0.05
<i>const</i>		0862470801	1.06 ± 0.11	2022-09	1.02 ± 0.05
$N_{\text{H}}$	$10^{22} \text{ cm}^{-2}$		9.5 (fixed)		9.5 (fixed)
$\Gamma^{\text{pow}}$			3.02 ± 0.25		3.22 ± 0.15
$F_{4.17-5.86 \text{ keV}}$	$10^{-13} \text{ erg s}^{-1} \text{ cm}^{-2}$		1.71 ± 0.12		2.16 ± 0.08
$E_{6.4 \text{ keV}}$	keV		6.4 (fixed)		6.4 (fixed)
$F_{6.4 \text{ keV}}$	$10^{-7} \text{ ph cm}^{-2} \text{ s}^{-1}$		< 8		5.3 ± 2.8
$\text{EW}_{6.4 \text{ keV}}$	keV		< 0.1		0.11 ± 0.02
$E_{6.7 \text{ keV}}$	keV		6.677 ± 0.015		6.663 ± 0.011
$F_{6.7 \text{ keV}}$	$10^{-6} \text{ ph cm}^{-2} \text{ s}^{-1}$		5.3 ± 0.7		5.7 ± 0.5
$\text{EW}_{6.7 \text{ keV}}$	keV		0.98 ± 0.08		0.90 ± 0.05
$\chi^2_{\text{red}}/\text{dof}$			0.93/82		1.06/305

term, chosen to be consistent with previous works, with fixed  $N_{\text{H}} = 9.5 \times 10^{22} \text{ cm}^{-2}$  according to T12; *pegpwrlw* – a power-law with normalization in 4.17–5.86 keV band and free photon index  $\Gamma$  linked between all observations; first Gaussian is 6.4 keV line with fixed energy 6.4 keV; second Gaussian describes 6.7 keV line with free energy. Both Gaussian components have width fixed at  $\sigma = 10 \text{ eV}$ . Note that we do not correct the iron line emission for the overall absorption (see Clavel et al., 2014, for explanation). The XMM-Newton 2020 and Chandra 2022 spectra were fitted separately. The best fitting parameters are listed in Table 2 and spectra are shown in Figs. 2-3. The equivalent width (EW) of iron lines have been estimated with SHERPA modeling and fitting package (Freeman et al., 2001; Siemiginowska et al., 2024), a part of the CIAO software (Fruscione et al., 2006). In XMM-Newton 2020 spectrum, the EW of 6.7 keV line was found at the level of  $\sim 1 \text{ keV}$ , while 6.4 keV line has not been significantly detected, and fitting procedure provided upper limit  $\text{EW}_{6.4 \text{ keV}} < 0.1 \text{ keV}$  (68% confidence level). Taking the last into account, we removed 6.4 keV line from the following XMM-Newton spectral analysis. The Chandra 2022 spectrum shows marginal detection of 6.4 keV line with  $\text{EW}_{6.4 \text{ keV}} \approx 0.1 \text{ keV}$ , consistent with XMM-Newton upper limit. Note that the spectral analysis of both 2020 and 2022 data sets demonstrate consistent model parameters.

Next, we extend the fitting energy range to 2–10 keV (1–9 keV) for XMM-Newton (Chandra) data, and include Arches cluster thermal emission modeled as optically thin, ionization equilibrium plasma (apec, Smith et al., 2001). The spectral model is defined as follows:

$$tbabs \times \text{const} \times (\text{apec} + \text{pegpwrlw}) \quad (2)$$

where *tbabs* denotes the TuebingenBoulder ISM absorption model (Wilms et al., 2000), and *pegpwrlw* is now defined in 2–10 keV band. Based on the previous observations of the Arches cluster (Wang et al., 2006, T12), we fixed the metallicity to  $Z = 1.7Z_{\odot}$  throughout the paper. Chandra 2022 spectrum shows clear excesses above the model at  $\sim 1.85$  and  $\sim 2.45 \text{ keV}$ , most likely corresponding to the  $K\alpha$  lines from He-like Si and S, respectively. To account for of these features observed in many studies of the Arches cluster (T12, Krivonos et al., 2017; Hua & Li, 2025), we added two Gaussian lines in the model. The best-fitting model parameters are listed in Table 3, while X-ray spectra are demonstrated in Figs. 4-5. The spectra of the Arches cluster in 2020 and 2022 are described by the model with acceptable fit statistics. The Arches thermal emission is described by plasma temperature  $kT \simeq 2 \text{ keV}$  and non-thermal excess is characterized by a hard continuum component. The total 2–10 keV flux is dominated by the low temperature component, and about one third of the observed flux can be attributed to the power-law. The photon index  $\Gamma$  measured with XMM-Newton in 2020 is determined with range  $[-0.8 \dots 1.5]$ . Chandra 2022 non-thermal component is described with power-law slope  $\Gamma \approx 1.5$  within range  $[0.6 \dots 2.6]$ , which is consistent with  $\Gamma = 1.1 \pm 0.7$  in the Arches cluster core obtained for the long XMM-Newton observation in 2015 (Krivonos et al., 2017), when X-ray intensity of the surrounding molecular cloud was significantly decreased, compared to 2000-2010.

To assess the significance of the power-law component detected with XMM-Newton 2020 (Chandra 2022) data, we repeated the fitting procedure without *pegpwrlw* term. As expected, the temperature of apec increased to a higher value of  $kT = 2.6 \pm 0.3 \text{ keV}$  ( $2.4 \pm 0.1 \text{ keV}$ ) and the quality of the fit worsened to

Table 3. Best-fitting parameters of apec and power-law model (Eq. 2).

Parameter	Units	XMM-Newton 2020		Chandra 2022	
		ObsID	Value	Epoch	Value
<i>const</i>		0862470701	1.0 (fixed)	2022-03	1.0 (fixed)
<i>const</i>		0862470601	$1.17 \pm 0.07$	2022-07	$1.04 \pm 0.03$
<i>const</i>		0862470801	$1.00 \pm 0.07$	2022-09	$1.02 \pm 0.03$
$N_{\text{H}}$	$10^{22} \text{ cm}^{-2}$		$12.5_{-1.2}^{+1.5}$		$11.7_{-0.6}^{+0.7}$
$kT$	keV		$2.09 \pm 0.25$		$2.16_{-0.18}^{+0.26}$
$Z/Z_{\odot}$			1.7 (fixed)		1.7 (fixed)
$I_{\text{apec}}$	$10^{-3}$		$1.69_{-0.32}^{+0.50}$		$1.77 \pm 0.35$
$\Gamma_{\text{pow}}$			$0.5_{-1.3}^{+1.0}$		$1.54_{-0.95}^{+1.06}$
$F_{2-10 \text{ keV}}^{\text{pow}}$	$10^{-13} \text{ erg s}^{-1} \text{ cm}^{-2}$		$1.33 \pm 0.63$		$2.24 \pm 0.65$
$F_{2-10 \text{ keV}}^{\text{total}}$	$10^{-13} \text{ erg s}^{-1} \text{ cm}^{-2}$		$4.91 \pm 0.18$		$5.94 \pm 0.13$
$E_{1.85 \text{ keV}}$	keV		—		$1.843_{-0.010}^{+0.016}$
$F_{1.85 \text{ keV}}$	$10^{-7} \text{ ph cm}^{-2} \text{ s}^{-1}$		—		$7.18_{-3.46}^{+3.68}$
$E_{2.45 \text{ keV}}$	keV		—		$2.424 \pm 0.022$
$F_{2.45 \text{ keV}}$	$10^{-6} \text{ ph cm}^{-2} \text{ s}^{-1}$		—		$1.11_{-0.28}^{+0.32}$
$E_{6.4 \text{ keV}}$	keV		—		6.4 (fixed)
$F_{6.4 \text{ keV}}$	$10^{-7} \text{ ph cm}^{-2} \text{ s}^{-1}$		—		$5.28 \pm 2.60$
$\chi^2_{\text{red}}/\text{dof}$			0.97/164		1.03/650

$\chi^2_{\text{red}}/\text{dof} = 1.05/166$  (1.1/652). The corresponding F-statistic test provides  $p$ -value of  $4 \times 10^{-4}$  ( $4 \times 10^{-11}$ ), which indicates that the power-law improves the fit.

The searches for the non-thermal spectral components are usually complicated by the observed degeneracy between the temperature of the thermal plasma and the slope and/or normalization of the non-thermal power-law<sup>1</sup> (e.g. Krivonos, 2022). In Fig. 6 we plot confidence contours for the power-law slope  $\Gamma$  and temperature of the thermal plasma, which shows the range of power-law slopes and corresponding  $kT$  values, acceptable by the data. To better constrain spectral components and break the degeneracy, the broad-band energy coverage is needed, especially above 10 keV.

## DISCUSSION

Deep Chandra observations of the Arches cluster in 2022 provide higher statistics above 7 keV, compared to XMM-Newton data in 2020, which allows us to better constrain the photon index of the power-law component ( $\Gamma \approx 1.5$  in range  $[0.6 \dots 2.6]$ ). This result is in line with detection of the non-thermal X-ray emission of the rich stellar cluster RMC 136 located in the starforming Doradus 30 complex (Feast et al., 1960) of the LMC by Sasaki et al. (2022) using eROSITA/SRG observations. The young (1.0-2.5 Myr) star cluster

RMC 136 hosts a rich population of massive stars with strong stellar winds (Brands et al., 2022), which makes it similar to the Arches cluster. With eROSITA/SRG, the X-ray spectrum of RMC 136 is well described with thermal emission from a non-equilibrium ionisation plasma ( $kT > 1$  keV) and non-thermal powerlaw with  $\Gamma = 1.3$ , indicating a hard X-ray spectrum, similar to the Arches cluster, as shown in the current work. This adds evidence to similar mechanism of particle acceleration in the shocks of the winds of massive stars in compact stellar clusters.

To constrain spatial extent of the Arches non-thermal emission in 2020, we constructed MOS1, MOS2 and pn combined sky image of the cluster in hard 8–12 keV band, as described in Sect. . As seen from the resulted sky mosaic (Fig. 7), the emission is well localized within the cluster core. According to the best-fitting spectral model (Eq. 2), the total flux is  $F_{8-12 \text{ keV}} = (1.1 \pm 0.3) \times 10^{-13} \text{ erg s}^{-1} \text{ cm}^{-2}$ , with relative contribution of apec and power-law components at the level of 26% and 74%, respectively.

The morphology of diffuse non-thermal emission is different from that was reported in Westerlund 1 (Muno et al., 2006) and Westerlund 2 (Bykov et al., 2023) where the emission apparently extended well beyond the cluster core. This difference can be understood, however, if the non-thermal emission is produced by the synchrotron radiation of very high energy electrons accelerated in the cluster core. In this case the extent of the synchrotron halo around the cluster would decrease with the increasing of the magnitude of the ambient magnetic field, surrounding a clus-

<sup>1</sup>It should also be noted that in some works, the authors use an additional thermal emission model with higher temperature, instead of a power law. This is quite reasonable, since the dense core of the Arches cluster contains Wolf-Rayet type stars and a large number of massive stars of early spectral classes, which allows us to expect the presence of plasma with higher temperatures.

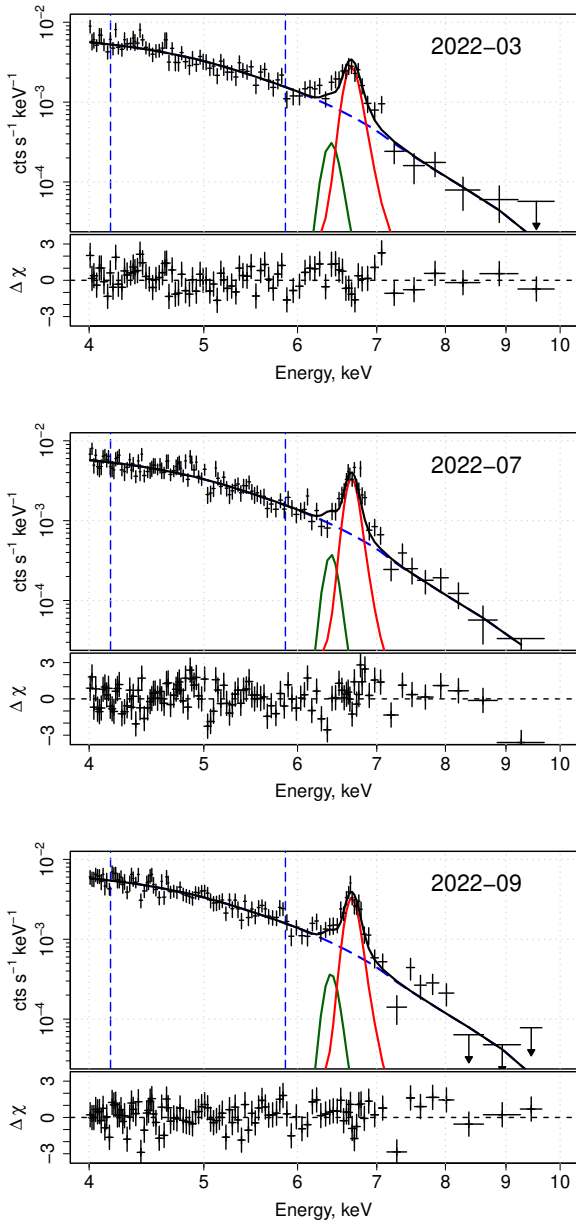


Fig. 3. Chandra X-ray spectra of the Arches cluster between 4 and 10 keV for three epochs in 2022. See Fig. 2 for reference.

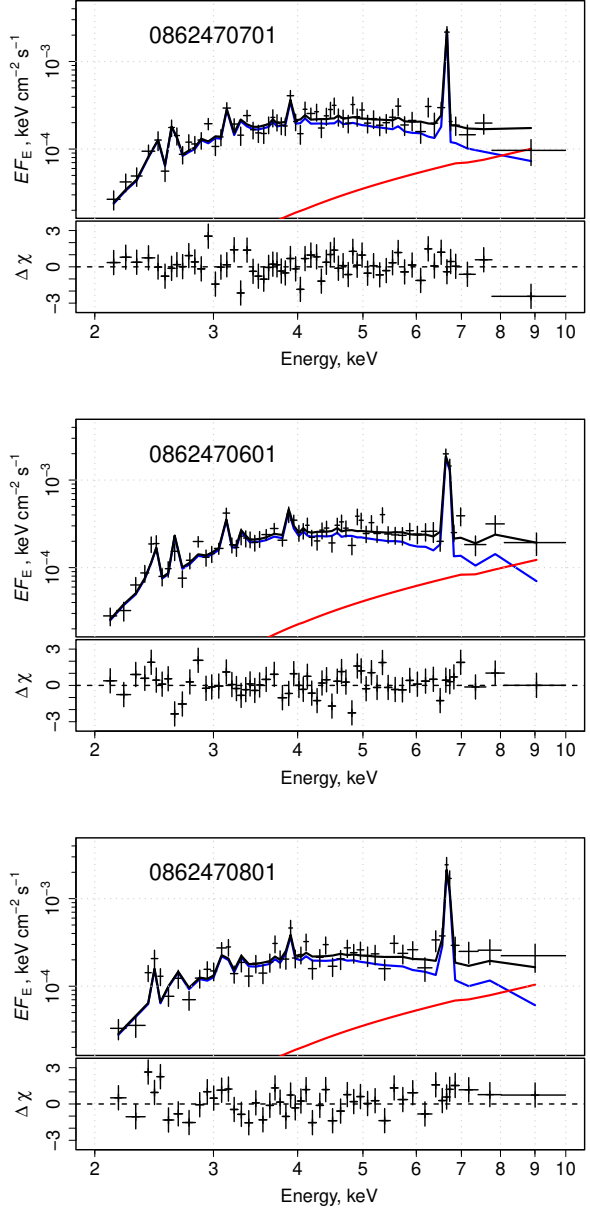


Fig. 4. Merged MOS1, MOS2 and pn X-ray spectra of the Arches cluster between 2 and 10 keV for three XMM-Newton observations in 2020. Best-fitting model (solid black line) is composed by a combination of an absorbed apec (blue) and power-law (red).

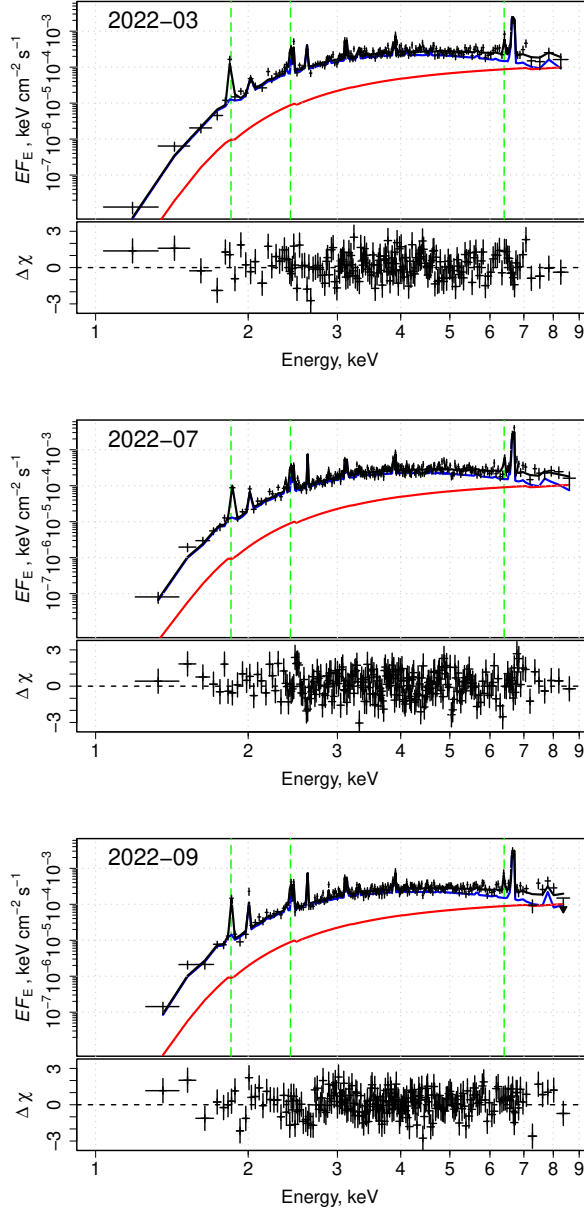


Fig. 5. Chandra 2022 X-ray spectra of the Arches cluster between 1 and 9 keV for three epochs in 2022. Best-fitting model (solid black line) is composed by a combination of an absorbed apec (blue) and power-law (red). Green dashed lines show positions of  $K\alpha$  lines of He-like Si at  $\sim 1.85$  keV, S at  $\sim 2.45$  keV and Fe at 6.4 keV (fixed), respectively, added to the fitting procedure (see Table 3).

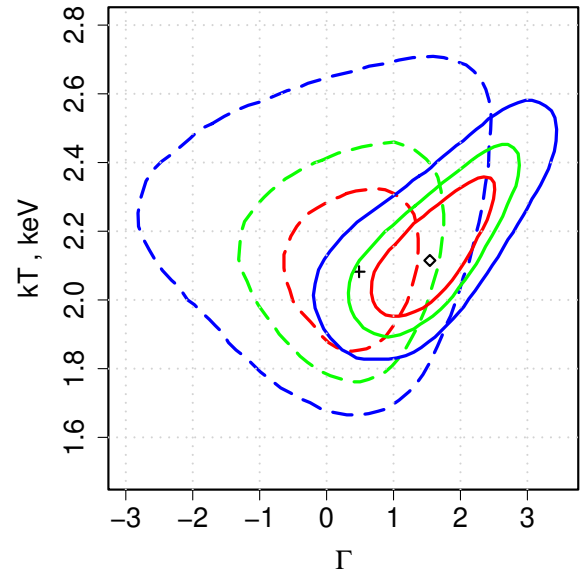


Fig. 6. Two-dimensional  $1\sigma$ ,  $2\sigma$  and  $3\sigma$  (red, green, blue colors) confidence contours for the slope  $\Gamma$  of the non-thermal component and the temperature of the thermal plasma in the 2–10 keV energy band for XMM-Newton 2020 and Chandra 2022 data sets shown as dashed and solid lines, respectively. Cross and diamond show best-fitting values for XMM-Newton 2020 and Chandra 2022 data, respectively.

ter. The mG range magnitude magnetic fields in the Galactic Center vicinity (see e.g. Akshaya & Hoang, 2024) are substantially higher than that expected at the other Galactic locations of the clusters and this reduce the size of the synchrotron halo of the Arches cluster. The localized morphology of the non-thermal emission helps us to distinguish it from the other non-thermal components present in the Galactic Center region.

#### SUMMARY AND CONCLUSIONS

In this work we characterize the X-ray emission of the Arches stellar cluster in a view of separating its thermal and non-thermal emission components. Previous studies have been concentrating on the reflected emission of the nearby molecular cloud. This emission, traced by the bright Fe  $K\alpha$  6.4 keV line, prevented detailed investigation of the intrinsic cluster's non-thermal emission, usually attributed to synchrotron or inverse Compton scattering of relativistic electrons. However, it should be noted that the compact core of the Arches cluster contains more than ten Wolf-Rayet stars and about one hundred massive stars of early spectral classes. This allows us to expect the presence of plasma with a temperature of 3–4 keV in certain regions of the cluster core. Therefore, in order to obtain a complete picture, it is necessary to clarify the spec-

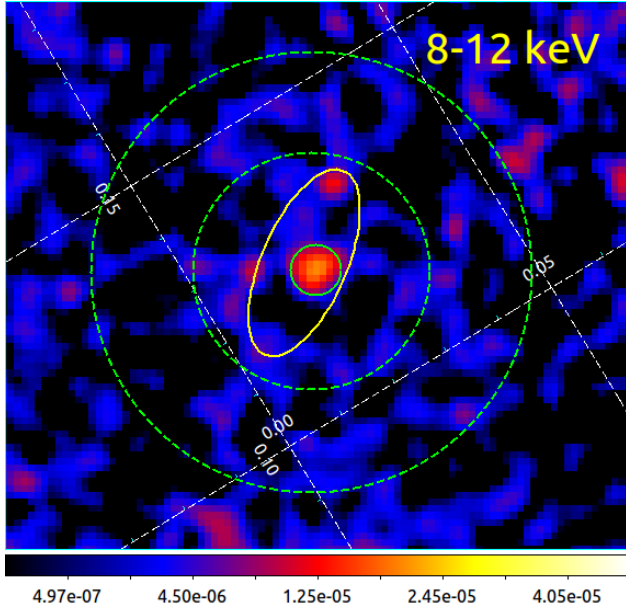


Fig. 7. XMM-Newton/EPIC exposure- and background- corrected map of the Arches cluster region in 8–12 keV range. For reference see Fig 1.

tral shape of the cluster’s emission at energies above 10 keV.

After significant decrease of the reflected emission, observed after 2015, we got a chance to observe Arches cluster in the cleanest environment. Using available deep XMM-Newton and Chandra observations of the cluster in 2020 and 2022, respectively, we demonstrated that Fe  $K\alpha$  6.4 keV line is not significantly detected within the cluster, providing evidence that contribution from the reflected emission of the molecular cloud is not significant. We showed that the overall X-ray spectral shape of the Arches cluster contains a soft, thermal component as well as a hard, non-thermal component. The spatial morphology of the latter is well localized in the cluster core region, and not extended beyond it.

## ACKNOWLEDGMENTS

RK acknowledges support from the Russian Science Foundation (grant no. 24-22-00212). MC acknowledges financial support from the Centre National d’Etudes Spatiales (CNES).

## REFERENCES

1. F. Aharonian, R. Yang, and E. de Oña Wilhelmi, *Nature Astronomy*, 3, 561 (2019)
2. M. S. Akshaya and T. Hoang, *Mon. Not. R. Astron. Soc.*, 531, 5012 (2024)
3. . (K. A. Arnaud), in G. H. Jacoby and J. Barnes (eds.), *Astronomical Data Analysis Software and Systems V*, Vol. 101 of *Astronomical Society of the Pacific Conference Series*, p. 17 (1996)
4. S. A. Brands, A. de Koter, J. M. Bestenlehner, P. A. Crowther, J. O. Sundqvist, J. Puls, et al., *Astron. Astrophys.*, 663, A36 (2022)
5. A. M. Bykov, Y. A. Uvarov, M. E. Kalyashova, D. V. Badmaev, I. Y. Lapshov, A. A. Lutovinov, et al., *Mon. Not. R. Astron. Soc.*, 525, 1553 (2023)
6. A. M. Bykov, *Astron. Astrophys. Rev.*, 22, 77 (2014)
7. R. Capelli, R. S. Warwick, N. Cappelluti, S. Gillessen, P. Predehl, D. Porquet, et al., *Astron. Astrophys.*, 525, L2 (2011a)
8. R. Capelli, R. S. Warwick, D. Porquet, S. Gillessen, and P. Predehl, *Astron. Astrophys.*, 530, A38 (2011b)
9. T. Chlebowski and C. D. Garmany, *Astrophys. J.*, 368, 241 (1991)
10. J. S. Clark, M. E. Lohr, F. Najarro, H. Dong, and F. Martins, *Astron. Astrophys.*, 617, A65 (2018a)
11. J. S. Clark, M. E. Lohr, L. R. Patrick, F. Najarro, H. Dong, and D. F. Figer, *Astron. Astrophys.*, 618, A2 (2018b)
12. J. S. Clark, M. E. Lohr, L. R. Patrick, and F. Najarro, *Astron. Astrophys.*, 623, A84 (2019)
13. M. Clavel, S. Soldi, R. Terrier, V. Tatischeff, G. Maurin, G. Ponti, et al., *Mon. Not. R. Astron. Soc.*, 443, L129 (2014)
14. A. S. Cotera, E. F. Erickson, S. W. J. Colgan, J. P. Simpson, D. A. Allen, and M. G. Burton, *Astrophys. J.*, 461, 750 (1996)
15. M. W. Feast, A. D. Thackeray, and A. J. Wesselink, *Mon. Not. R. Astron. Soc.*, 121, 337 (1960)
16. D. F. Figer, S. S. Kim, M. Morris, E. Serabyn, R. M. Rich, and I. S. McLean, *Astrophys. J.*, 525, 750 (1999)
17. D. F. Figer, F. Najarro, D. Gilmore, M. Morris, S. S. Kim, E. Serabyn, et al., *Astrophys. J.*, 581, 258 (2002)
18. . (P. Freeman, S. Doe, and A. Siemiginowska), in J.-L. Starck and F. D. Murtagh (eds.), *Astronomical Data Analysis*, Vol. 4477 of *Society of Photo-Optical Instrumentation Engineers (SPIE) Conference Series*, pp 76–87 (2001)
19. . (A. Fruscione, J. C. McDowell, G. E. Allen, N. S. Brickhouse, D. J. Burke, J. E. Davis, et al.), in D. R. Silva and R. E. Doxsey (eds.), *Observatory Operations: Strategies, Processes, and Systems*, Vol. 6270 of *Society of Photo-Optical Instrumentation Engineers (SPIE) Conference Series*, p. 62701V (2006)
20. Z. Hua and Z. Li, *Mon. Not. R. Astron. Soc.*, 540, 3850 (2025)
21. P. J. Kavanagh, *Ap&SS*, 365, 6 (2020)
22. R. A. Krivonos, J. A. Tomsick, F. E. Bauer, F. K. Baganoff, N. M. Barriere, A. Bodaghee, et al., *Astrophys. J.*, 781, 107 (2014)

23. R. Krivonos, M. Clavel, J. Hong, K. Mori, G. Ponti, J. Poutanen, et al., *Mon. Not. R. Astron. Soc.*, 468, 2822 (2017)
24. R. A. Krivonos, *Astronomy Letters*, 48, 636 (2022)
25. E. Kuznetsova, R. Krivonos, M. Clavel, A. Lutovinov, D. Chernyshov, J. Hong, et al., *Mon. Not. R. Astron. Soc.*, 484, 1627 (2019)
26. F. Marin, E. Churazov, I. Khabibullin, R. Ferrazzoli, L. Di Gesu, T. Barnouin, et al., *Nature*, 619, 41 (2023)
27. M. P. Muno, C. Law, J. S. Clark, S. M. Dougherty, R. de Grijs, S. Portegies Zwart, et al., *Astrophys. J.*, 650, 203 (2006)
28. M. Sasaki, J. Knies, F. Haberl, C. Maitra, J. Kerp, A. M. Bykov, et al., *Astron. Astrophys.*, 661, A37 (2022)
29. E. Serabyn, D. Shupe, and D. F. Figer, *Nature*, 394, 448 (1998)
30. A. Siemiginowska, D. Burke, H. M. Günther, N. P. Lee, W. McLaughlin, D. A. Principe, et al., *ApJS*, 274, 43 (2024)
31. R. K. Smith, N. S. Brickhouse, D. A. Liedahl, and J. C. Raymond, *Astrophys. J. (Letters)*, 556, L91 (2001)
32. S. L. Snowden, M. R. Collier, and K. D. Kuntz, *Astrophys. J.*, 610, 1182 (2004)
33. S. L. Snowden, R. F. Mushotzky, K. D. Kuntz, and D. S. Davis, *Astron. Astrophys.*, 478, 615 (2008)
34. G. Stel, G. Ponti, F. Haardt, and M. Sormani, *Astron. Astrophys.*, 695, A52 (2025)
35. V. Tatischeff, A. Decourchelle, and G. Maurin, *Astron. Astrophys.*, 546, A88 (2012)
36. L. K. Townsley, P. S. Broos, G. P. Garmire, and M. S. Povich, *Astrophys. J. Suppl. Ser.*, 244, 28 (2019)
37. M. Tsujimoto, Y. Hyodo, and K. Koyama, *PASJ*, 59, 229 (2007)
38. D. A. Verner, G. J. Ferland, K. T. Korista, and D. G. Yakovlev, *Astrophys. J.*, 465, 487 (1996)
39. A. Vikhlinin, R. A. Burenin, H. Ebeling, W. R. Forman, A. Hornstrup, C. Jones, et al., *Astrophys. J.*, 692, 1033 (2009)
40. Q. D. Wang, H. Dong, and C. Lang, *Mon. Not. R. Astron. Soc.*, 371, 38 (2006)
41. J. Wilms, A. Allen, and R. McCray, *Astrophys. J.*, 542, 914 (2000)
42. F. Yusef-Zadeh, C. Law, M. Wardle, Q. D. Wang, A. Fruscione, C. C. Lang, et al., *Astrophys. J.*, 570, 665 (2002)

Latex style was created by R. Burenin